
Article:

Homoky, WB orcid.org/0000-0002-9562-8591, Conway, TM, John, SG et al. (4 more authors) (2021) Iron colloids dominate sedimentary supply to the ocean interior. Proceedings of the National Academy of Sciences of USA, 118 (13). e2016078118. ISSN 0027-8424

https://doi.org/10.1073/pnas.2016078118

Title page

Iron colloids dominate sedimentary supply to the ocean interior

William B Homoky[a][b][1], Tim M Conway[c], Seth G John[d], Daniela Koenig[e], FeiFei Deng[b], Alessandro Tagliabue[e], Rachel A. Mills[f]

[a]University of Leeds, School of Earth and Environment, UK
[b]University of Oxford, Department of Earth Sciences, UK
[c]University of South Florida, College of Marine Science, USA
[d]University of Southern California, Department of Earth Sciences, USA
[e]University of Liverpool, School of Environmental Sciences, UK
[f]University of Southampton, School of Ocean and Earth Science, UK

[1] To whom correspondence should be addressed. Email: W.Homoky@leeds.ac.uk

Abstract

Dissolution of marine sediment is a key source of dissolved iron (Fe) that regulates the ocean carbon cycle. Currently, our prevailing understanding, encapsulated in ocean models, focuses on low oxygen reductive supply mechanisms and neglects the emerging evidence from iron isotopes in seawater and sediment porewaters for additional non-reductive dissolution processes. Here we combine new measurements of Fe colloids and dissolved δ^{56}Fe in shallow porewaters spanning the full depth of the South Atlantic Ocean to demonstrate that it is lithogenic colloid production that fuels sedimentary iron supply away from low oxygen systems. Iron colloids are ubiquitous in these oxic ocean sediment porewaters and account for the lithogenic isotope signature of dissolved Fe (δ^{56}Fe = +0.07±0.07‰) within and between ocean basins. Isotope model experiments demonstrate that only lithogenic weathering in both oxic and nitrogenous zones, rather than precipitation or ligand-complexation of reduced Fe species, can account for the production of these pore water Fe colloids. The broader covariance between colloidal Fe and organic carbon (OC) abundance suggests that sorption of OC may control the nano-scale stability of Fe minerals by inhibiting loss of Fe(oxyhydr)oxides to more crystalline minerals in the sediment. Oxic ocean sediments can therefore generate a large exchangeable reservoir of organo-mineral Fe colloids at the sediment water interface (a “rusty source”) that dominates benthic supply of dissolved Fe to the ocean interior, alongside reductive supply pathways from shallower continental margins.

Keywords: ocean sediment; porewater; iron isotope; iron colloid; iron organo-mineral

Significance statement

Phytoplankton assimilate carbon dioxide, produce oxygen and nourish food webs on a scale that impacts planetary processes but are limited by iron deficiency over much of the global surface ocean. Therefore, we must understand processes that regulate the ocean's iron inventory to accurately simulate and predict the ocean's response to change. This study reveals that the widespread production of nano-sized iron colloids from the weathering of lithogenic material drives sedimentary iron supply throughout the deep ocean. The discovery accounts for the unexplained occurrence of colloids and patterns of iron isotope variation previously observed in other parts of the deep ocean, and suggests how long standing assumptions we have used to simulate iron supply in ocean models must be revised.

Introduction

Sediments undergo early diagenetic transformations that are understood to provide an important source of dissolved iron (dFe) to the ocean that is used to fuel primary production and secondary food webs, fix nitrogen and support the air-sea transfer of carbon dioxide (1, 2). Nevertheless, fundamental questions remain concerning the magnitude of dFe released from ocean sediments, and the mechanisms through which this supply may be moderated. Such uncertainty is most acute in oxic and deep-water regions, which bear the fewest observations, but represent the largest area of the ocean sediment-water interface (3). Here, comparatively small sedimentary releases of dFe have the cumulative-potential to enhance the dFe inventory of the deep ocean and – in so far as it connects with surface water – relieve iron-deficiency for phytoplankton. Porewaters in these deep water regions maintain a persistently oxic and/or nitrogenous state adjacent to bottom waters that is largely unexamined for its role in the marine iron cycle. These gaps in knowledge hinder our ability to make more accurate simulations of the carbon cycle in ocean biogeochemical models (4).

Two principle processes are thought to be driving Fe dissolution from sediments that underpin the magnitude and variability of dFe inputs to the ocean. The first is a reductive-dissolution (RD) process which demonstrably occurs during early diagenetic oxidation of organic carbon (OC) and produces high abundances of reduced, soluble and isotopically light Fe in ferruginous porewaters generally beneath the Fe-oxidising fronts of nitrous oxides and oxygen (5-7). The second is a non-reductive dissolution (NRD) process to account for the comparatively unfractionated or heavy isotope compositions of dFe attributed to sedimentary inputs in some oxygenated regions of the open ocean (8) and in the oxic zones of marine sediment porewaters (9), but the mechanisms governing so-called NRD in oxic sediments are unclear.

Reductive dissolution of Fe is coupled to organic carbon oxidation and is widely observed in shallow porewater in sediments with high oxygen consumption rates, under productive shelf seas, near zones of upwelling and overlain by oxygen-depleted seawater (10). Low seawater oxygen content serves to enhance the efflux of reduced and soluble Fe (sFe; filtered <0.02 μm) from ferruginous pore waters and enables sFe(II) to propagate further in the water column (11-14). Subsequently, without sufficient chelation by organic ligands sFe(II) will be lost to oxidative precipitation (7, 15, 16) scavenging (12) and sedimentation in deeper water (16, 17). Sedimentary RD provides a key component of the ocean's dFe inventory that is most pronounced in the upper ocean (1, 10, 11, 13). It is also the only mechanism by which most ocean biogeochemical models simulate the sedimentary release of dFe (4), since model parameterisations rely on empirical relationships between dFe fluxes, OC oxidation rates, bottom water oxygen contents, and/or water depth (1, 11, 18, 19).

Non-reductive dissolution (NRD) is a term previously used to describe a sedimentary source of isotopically heavy dFe to the water column (8), and has since been used to describe the presence of lithogenic isotope compositions observed in oxidizing zones from some deep ocean sediment porewaters (9). Similar observations have become commonplace in the ocean interior (20-23), such that non-reductive sedimentary processes appear to be important for the ocean's dFe inventory. However, the detection of lithogenic dFe isotope signatures in porewaters (6, 9), within western North Atlantic benthic nepheloid layers, and in the water-column far from sediment sources have been difficult to explain (24). The role played by this additional source of dFe is not yet included in global ocean models.

Based on the very low solubility of silicate minerals and Fe(III) oxides in circumneutral pH and oxygenated seawater, NRD ought to be incapable of sustaining a benthic flux of dFe to the ocean without significant chelation by organic ligands (25). Due to a strong isotope fractionation effect, however, ligand complexation of Fe would produce a much heavier Fe isotope signal in the ocean (26), which is at odds with the isotopic evidence for NRD (20-23). To reconcile these differences between NRD theories and dissolved Fe isotope observations we ought to consider any physico-chemical partitioning within the dFe pool. The dissolved measurement of Fe (dFe; $<0.2\ \mu$m) and dFe isotopes, may reflect variable contributions of ligand-bound and soluble Fe(II/III) (sFe; $<0.02\ \mu$m) and larger mineral or organo-mineral forms of colloidal Fe (cFe; 0.02 to 0.2 μm) in the ocean (23, 27). Such components of the dFe pool are often unaccounted for and have been neglected in previous studies reporting the occurrence of sedimentary NRD in the water column. However, sizable concentrations of colloidal Fe (10^1 μmoles L^{-1}) have been observed in oxic-nitrogenous porewaters from deep ocean turbidites of the Southern Ocean, where dFe isotope compositions also matched the solid phase inputs from ocean island basalt. Whether these colloids formed *in situ* through organic complexation, and/or as secondary minerals from either reductive or non-reductive processes was unresolved. A comparison to fresh tephra layers in the Caribbean Sea showed that ocean island basalt weathering and production of nanoscale ferrihydrite or Fe-bearing smectite clays were thermodynamically plausible explanations for cFe in the Southern Ocean porewaters (28). Recently, Klar *et al.*, (7) looked for Fe colloids in porewaters from a shallow shelf sediment, but found few if any, and that the porewaters were dominated by light dFe isotope signatures and sFe(II) attributable to RD by bacteria. Previous studies have not resolved where or why cFe occurs in sediment porewaters of the continental shelf-slope-basin transition, or the extent to which they may influence the inventory and isotope composition of dFe input to the ocean (20, 22). These lessons need to be learned by examining the soluble and colloidal partitioning of dissolved Fe in porewaters and comparing them to dissolved Fe isotope signatures from a wider range sedimentary carbon and oxygen regimes in the ocean environment.

Without appropriate simulation of this dFe source, ocean biogeochemical models will fail to represent spatial patterns in dFe flux from the seafloor, the response of these fluxes to changing ocean environments, and their consequences for ocean biogeochemistry. Confounding this issue is the omitted role of advective transport mechanisms, internal waves and benthic boundary layers that will facilitate exchanges between oxic sediments and the ocean interior(3, 29, 30). To make progress on this important issue requires new understanding on the mechanisms by which Fe dissolves and is supplied to the ocean by oxic sediments.

Herein, we present findings from surface sediment cores from sites that span the depth and breadth of the Southwest Atlantic Ocean. The UK-led GEOTRACES expedition, GA10W, recovered porewaters in 2011 from the Uruguayan continental shelf, slope, Argentine abyssal floor and Mid-Atlantic Ridge (SI Appendix, Table S1). We report porewater dFe isotope compositions and further evidence of the physico-chemical partitioning of dFe between soluble and colloidal size fractions (where cFe = dFe-sFe) at selected locations and depths where porewater inventories of Fe were sufficient to permit these determinations. We apply principles of isotope fractionation and mass-balance across the dissolved and soluble size classes to test hypothetical controls on the dFe pool in these porewaters. Our study reveals that oxidizing zones of marine sediments are important regions of non-reductive cFe production derived from lithogenic material, which ultimately determine the dFe inventory and isotope composition supplied to the deep ocean.

Results

South Atlantic sediment compositions. Between the deepest abyssal station of GA10W (18) to the shallowest shelf-top station (24) core top sediments were composed almost entirely of lithogenic material (84 to >99%; Figure 1; averages from 0-5cmbsf, SI Appendix, Table S2) – consistent with continental weathering input and dispersion to the shelf, slopes and abyssal floor of the Argentine Basin (*Cf.* Weijer et al., (31)). Lithogenic material was the second most significant component of core-top material (17%) at the most distal station located on the Mid-Atlantic Ridge, Station 8, more than 3500km from the continental margin along the path of the South Atlantic Current, and above the likely calcite saturation horizon (32). Station 8 was predominantly biogenic carbonate (82%), with trace amounts (<1%) of biogenic opal, whereas stations 18 to 24 contained at most only modest amounts of opal (up to 14%) and carbonate (up to 8%). There was a gradient in total organic carbon (TOC) content from a mid-slope maximum (3.9%, station 22) - coincident with a mid-slope peak in pelagic components - down to minimum values on the permeable sandy shelf (0.2%, station 24) and across the basin on the Mid-Atlantic Ridge (0.2%, station 8).

Dissolved porewater contents. Porewater O_2 was depleted from bottom water values and was observed to penetrate between 0.4 and >9 cm below the seafloor (cmbsf) across all sites. There was a strong exponential relationship between calculated rates of C oxidation (determined from O_2 flux), and water depth (SI Appendix, Fig. S1 and Table S3). Other such indicators of early diagenetic cycling in porewaters had equivalent water depth dependence between stations.

Porewater nitrite+nitrate (herein after termed nitrous oxides) were depleted down core from bottom water values (SI Appendix, Fig. S2) and coincided with increased ammonia concentrations (SI Appendix, Table S4). Taken together, these data indicate the reductive cycling of nitrous oxides to ammonia in a nitrogenous zone underlying the oxic surface layer. All stations contained sub-surface maxima in dissolved manganese (dMn) and dFe, up to 10 and 52 μM, respectively, consistent with the reductive-dissolution of these metals that has been observed beneath oxic-nitrogenous zones elsewhere in deep-sea sediments (e.g. (9, 33)). A single exception was station 8, where nitrous oxides were not obviously depleted, and where neither dMn nor dFe maxima were observed (SI Appendix Fig. S2 and Table S5).

Porewater δ^{56}Fe of dFe maxima averaged -0.93±0.2‰ (1 SD, *n* = 5) between stations 18 and 24 (SI Appendix, Fig. S2), and were isotopically lighter than average igneous crustal material at δ^{56}Fe = +0.09‰ (34). Light dFe isotopic compositions shifted to heavier values down core and exceeded the average isotopic composition of the crust beneath the ferruginous zones of stations 23 and 22 (up to a maximum of +0.63‰). Nearly all stations contained porewater concentrations of dFe in the surface oxic-nitrogenous zones 10 to 500 times higher than background seawater concentrations with δ^{56}Fe (+0.07±0.07‰, *n* = 11) indistinguishable from average crustal rocks. A single exception was station 23, where ferruginous conditions extended into the upper centimetre of the sediment and a light dFe isotope composition was observed (-1.37‰).

Soluble and colloidal partitioning of dissolved Fe in porewaters. A comparison of soluble (<0.02μm) and dissolved (<0.2μm) porewater filtrates at stations 8, 18, 21 and 22 indicates that sub-surface maxima in dMn and dFe concentration were almost exclusively due to the presence of soluble and most likely reduced species of the metals (Fig. 2; SI Appendix, Table S5; *Cf.* (7)). However, porewater also contained significant detectible quantities of dFe (between 0.01 and 0.5 μM) that was far in excess of sFe throughout the overlying nitrogenous and oxic zones. Therefore, between 17±6 and 99±3% of dFe in oxic-nitrogenous porewater was in a colloidal size-class (0.02 to 0.2 μm; Fig. 2). To a lesser but significant extent, dMn also occurred as colloids in the oxic porewater (between 0 and 61±5 %; SI Appendix, Table S5).

Discussion

Early diagenesis of Fe and Mn. High proportions of lithogenics relative to pelagic material on the Uruguayan margin and deep Argentine Basin compared to the Mid-Atlantic Ridge, (Fig. 1) broadly match regional sediment classifications in a recent census of the seafloor, which indicates these sites are also typical of many other margin, basin and ridge environments of the global ocean (35). Calculated fluxes of O_2 in cohesive sediments from the upper shelf slope (St 23) to Mid Atlantic Ridge (St 8), and the relationship of these fluxes to water depth (SI Appendix, Fig. S1), follow an expected gradient in the amount of OC that survives remineralisation in the water column and enters the sediment to fuel early diagenetic reactions (36). Porewater properties reported here may therefore provide a suitable analogue for other oxygenated shelf-slope-basin transitions of the global ocean.

Porewater concentration profiles provide evidence for a common down core sequence of electron acceptor cycling in the order O_2>NO_x>Mn^{4+}>Fe^{3+}>SO_4^{2-}, which follows the Gibbs free energy available to the bacteria which catalyse these reduction-oxidation pathways (37). The soluble nature of dFe and dMn maxima (SI Appendix, Fig. S2) is evidence for the reduced species of these metals accumulating in porewaters (*c.f.* (7)). The light isotopic composition of dFe in these ferruginous zones matches previous findings too, where reductive-dissolution of Fe(III)oxyhydroxides to soluble $Fe(II)_{(aq)}$ was also reasoned to account for similar light δ^{56}Fe values (5-7, 9, 11, 38, 39), and is supported by experiments (40, 41). However, our novel investigation of the oxic-nitrogenous zones provides evidence for a previously undocumented reservoir of colloidal Fe (cFe) in continental slope and basin sediment porewater of the South Atlantic Ocean (Fig. 2). These colloids will play a crucial role in regional Fe supply, particularly in deep waters, and their occurrence signifies that they are likely to be prevalent in other oxygenated slope and basin environments.

The occurrence of Fe colloids in sediment porewater. Iron colloids occur commonly in the ocean (23, 27, 42). Most often they are attributed to organic complexation of Fe(III) (43, 44) or nano-particulate Fe(oxyhdr)oxide, clay (45-47) or occasionally Fe sulphide (48) minerals. Recent findings indicate deep Atlantic Ocean waters contain cFe that originates from the seafloor (27), but there are comparatively few assessments of cFe in marine sediment porewaters beyond those presented and discussed in this article (6, 7, 28).

Our study shows that the occurrence of cFe in surface sediment porewater is extensive and, thus far, ubiquitous in oxic deep-ocean lithogenic sediments. What is more, these colloids share a nearly identical Fe isotope composition throughout the ocean: in porewaters where dFe has been shown to comprise between 70 and 100% cFe, the dFe isotope composition (+0.12±0.07‰, n = 24) remains indistinguishable from the δ^{56}Fe of the average igneous weathering product (+0.09‰ (34); Fig. 3). It stands to reason that a common mechanism must be responsible for the formation of cFe from lithogenic material in oxidising environments, which can operate independently of RD driven by bacteria to account for this isotopic uniformity between cFe and lithogenics.

The Fe isotope composition of igneous rocks is reflected in its detrital weathering and oxidation product (49, 50). We expect sediments derived from different igneous rocks with different histories of siliciclastic cycling to exhibit variable rates of seafloor weathering, dissolution and authigenesis (3, 9, 51, 52). Accordingly, the porewater content of cFe reported from young deep-ocean Crozet Island Basalt is greater than we report here for the South Atlantic, even for basaltic sites with comparatively low TOC (Fig. 2b). In the present study however, between sites that share a similar lithogenic provenance, we see a strong positive correlation between mean cFe concentration in oxidising porewater and the mean core-top abundance of TOC (r = 0.962 p = 0.04, n = 4; Fig. 2b). Taken together, these igneous and organic relationships reinforce the view that cFe is controlled by the weathering of lithogenic detritus and that OC may be required for the stabilisation of cFe we observe in the porewaters. For example, OC sorption to oxyhydroxide mineral surfaces can inhibit Fe transformation into more crystalline and refractory minerals. This interaction is evidenced experimentally (53), and by observations that show that one fifth of marine sedimentary OC is bound to reactive Fe phases (54), which are predominantly nano-scale oxyhydroxides in marine sediment oxic layers (47). Therefore, Lalonde *et al.*'s (54) proposition of a "rusty sink", in which formation of meta-stable Fe(III) organo-minerals promotes OC burial, may here prove to be a "rusty source" mechanism for the occurrence of cFe in oxic porewater. In other words, our assessment of core-top TOC and cFe content could reflect the availability of OC compounds formed during organic matter degradation and that are suited to stabilisation of nano-scale Fe oxyhydroxide.

Mechanisms governing the production of porewater Fe solutes and mineral colloids. It is important to determine whether cFe in oxidising porewater is an authigenic precipitate of Fe produced by RD or if it has formed by a distinctly non-reductive pathway, because these processes of colloid production (or within our operational definitions here, sediment-dissolution) will have different drivers and impacts in the ocean and may respond and feed back differently to changes in the overlying ocean environment. Addressing this issue is essential if we are to build confidence in the paradigms we depend upon to estimate the size and variability of iron inputs in ocean biogeochemical models (3, 4, 18).

We can simulate the steady-state porewater production/consumption profiles needed to reproduce measured soluble, dissolved, and colloidal Fe concentration profiles across an oxic-nitrogenous zone. Of the GA10W transect, Station 21 offers uniquely detailed data resolution to perform this assessment with the 1-dimensional steady-state "Rate Estimates from Concentration profiles" or REC model previously described by Lettman *et al.* (55). If we impose a lower boundary condition for sFe and dFe concentrations equal to porewater values at 9.5 cmbsf, and a surface boundary condition of 1 nmol L^{-1} to approximate bottom water (24), model fits to sFe and dFe data (and cFe by difference) may be calculated (Fig. 4).

The sFe profile is reproduced with a single region of production in the ferruginous zone (>7.5 cmbsf) and a single region of consumption above it (5-7.5 cmbsf) in accordance with the oxidising potential of nitrous oxides. A more complex production profile is required to simulate dFe, which is predominantly determined by the production of cFe rather than sFe. Production of cFe coincides with a region of sFe consumption (between 5 and 7.5 cmbsf), indicating sFe-oxidation could partially contribute an authigenic source to cFe in porewater. However, the dFe profile requires similar magnitudes of cFe production in oxic, nitrogenous, and ferruginous zones. Therefore, sFe oxidation alone does not fully account for the production of cFe.

Porewater isotopic constraints on the genesis of colloidal Fe. We can further test hypothetical controls on the genesis of cFe using an isotopic mass-balance model. We consider two scenarios in which the isotopic composition of dFe is determined by theoretical controls on soluble and colloidal Fe species: In the first scenario, sFe (assumed here to be $Fe(II)_{aq}$) is oxidised and isotopically fractionated, and cFe is assumed to form entirely from the authigenic products of sFe oxidation. In the second scenario, sFe is oxidised and isotopically fractionated, but removed to the sediment, and cFe is formed entirely from the oxidative weathering of lithogenic material without any Fe isotope fractionation. Initial isotope ratios for sFe and cFe can be adjusted so that the resultant dFe isotope ratio matches the observed value at the dFe maxima 9.5 cmbsf. The isotope compositions of sFe and authigenic cFe can then be determined by an isotope fractionation factor (α) during $Fe(II)_{aq}$ oxidation. Herein we choose to evaluate values of α <1 and >1, such that $\Delta_{sFe\text{-}cFe}$ was ±0.5‰ (SI Appendix, SI Text 2).

By modelling these idealised controls on the isotopic composition of porewater dFe, we make two interesting observations. Firstly, porewater dFe isotopes cannot be reproduced when oxidation of sFe determines the isotope composition of cFe (Figure 5ab), whereas dFe isotopes are reproduced quite well when cFe reflects a homogenous crustal weathering product (Figure 5cd). Secondly, dFe isotopes are most accurately reproduced at the transition between ferruginous and oxic-nitrogenous conditions (i.e. region of maximum sFe consumption; *c.f.* Fig. 4) when α is <1. We achieve our best simulation of porewater dFe isotopes when cFe is lithogenic and sFe is consumed by oxidation with α of 0.9995 (Figure 5d).

We note that the nature of authigenic mineral sinks linked to sFe oxidation will be more complex than has been represented in our simplified approach to isotopic mass-balance above. For example, sFe oxidation may be catalysed by NO_3-reducing Fe(II)-oxidizing bacteria - most prevalent in marine sediments with low to moderate TOC content (56). Siderite ($Fe(II)CO_3$) is also a common authigenic precipitate of $Fe(II)_{aq}$ that produces kinetic and equilibrium isotope effects ($Fe(II)_{aq}$-$FeCO_3$ = Δ+1.2 and 0.0 ‰, respectively (57).

Crucially, however, authigenic Fe minerals must either preserve or fractionate isotope ratios from their source of aqueous Fe(II). If Fe(II) is produced from ferruginous depths in porewater following conventional RD theory then any such authigenic minerals must either preserve (e.g. *via* siderite) or fractionate (e.g. *via* oxidation to ferrihydrite) the light isotope composition of the Fe(II) supplied from the ferruginous zone. Because we have chosen to consider a range of α values (from 0.9995 to 1.0005), our simulations may represent a wide range of potential isotope fractionations that might reasonably be achieved by formation of common authigenic Fe minerals (40, 41, 57, 58) or by complexation of soluble Fe with organic ligands (26, 50). Yet we still determine colloidal Fe isotopes to be almost uniformly identical to the continental crust, within and between ocean basins. This occurs in the presence of contrasting sediment composition (e.g. opaline, carbonate, basaltic, siliciclastic and TOC content) between sites. Such compositional variability would theoretically encourage variations in the solubility of different authigenic phases, and therefore impart different isotope fractionation effects upon $Fe(II)_{aq}$ between sites, but this variability in the cFe pool is simply not observed (Fig. 3). For these reasons we consider that cFe is principally formed by oxidative weathering of lithogenic material without dissimilatory reduction and isotope fractionation by bacteria. While bacterial siderophores may promote Fe oxide and Fe-bearing silicate mineral dissolution, they can do so indirectly via proton-promoted dissolution (59), which does not fractionate Fe isotopes (60). We posit that nano-scale ferrihydrite produced by oxidative weathering is further stabilised by the sorption of OC, but sorption to the Fe mineral surface imparts no fractionation effect and therefore preserves its Fe isotope composition.

Implications for the ocean Fe inventory. A lithological source of Fe colloids in surface oxidising porewater has important implications for our assessment of benthic Fe supply to the ocean. The oxidising conditions reported here reflect those that occur commonly below the sediment-water interface of major open ocean margins and basins (36). Thus we provide key new evidence to further disqualify the assumption that only RD controls benthic input of dissolved iron to the ocean (8, 9). Organo-mineral Fe weathering products with a longer oceanic residence time than reduced Fe species may explain how dFe bearing non-reductive crustal isotopic signatures can escape the seafloor and be transported to the ocean interior.

The resultant flux of lithogenic Fe colloids to the ocean will reflect the balance of *in situ* production rates and benthic exchange mechanisms (Fig. 6). We find that the absolute abundance of cFe in porewater remains greatest in sediments composed of fresh basaltic weathering products, likely indicative of the higher Fe and Mn contents of mafic source rocks and the susceptibility of mafic minerals (e.g. basalt glass, olivine, amphibole) to weather rapidly and produce Fe(oxy)hydroxides and clays during marine early diagenesis (*c.f.* Fig. 2b). We also find that OC is an important additional factor in the production of cFe, but we can only speculate as to the nature of OC moieties in porewater that might elicit the strong cFe relationship with TOC observed in South Atlantic sediments. We suggest that degradation of organic matter may yield bacterial communities and compounds with functional groups suited to (a) enhance the oxidative weathering Fe oxide and Fe-bearing silicate minerals (59), and (b) the sorption of Fe(oxyhy)oxides present in oxic zones (61), which inhibits the loss of Fe to more crystalline phases and encourages preservation as nano-minerals (54). If so, then seafloor organic carbon supply may still exert an important overarching influence on sedimentary dFe fluxes to the ocean, only here it is due to enhanced non-reductive dissolution and mineral-protection effects, rather than reductive dissolution or ionic complexation processes that fractionate Fe isotopes (5, 26).

Benthic exchange mechanisms will promote the flux of cFe produced by seafloor weathering and OC complexation to the ocean interior (Fig. 6). Established gradients in cFe concentration between porewater and bottom water may promote a diffusive flux of colloids towards the deep ocean. Without knowledge of cFe diffusion coefficients, diffusive flux calculations may inaccurately need to assume their behaviours match those of the aqueous ion. On the other hand, the stability of organo-mineral colloids in the presence of oxygen means that large reactive losses, such as those required to account for oxidation of aqueous Fe(II) (7, 12), may not be applicable to an assessment of cFe (28). Of further significance, biophysical activity and bottom shear stress will promote the entrainment of surface sediment and porewaters in the ocean (46, 62). These entrainments can encourage the scavenging-removal of aqueous Fe(II) and Fe(III) species present in excess of ligand concentrations (e.g. (12)), and simultaneously promote the exchange of mineral solids (including colloids) between the sediments and the water column (27, 29). Energy for the generation and transport of a benthic nepheloid inventory appears unevenly in the ocean. It is tied to upper ocean dynamics and the internal tide and is compounded by bathymetric roughness, island mass effects and reflection angles (29, 63, 64). Despite complexity to these interactions, their importance for boundary exchange and transport in the ocean is well recognised (16, 30) and even evidenced to facilitate the supply of cFe (23, 27) and lithogenic Fe isotopes to the water column (20) (Fig. 6).

Where sites of maximum cFe production and potential benthic entrainment overlap, conditions suited to produce a flux of cFe and crustal isotope signatures to the ocean ought to be optimised (Fig. 7). Improved knowledge of where cFe fluxes occur would assist their inclusion in new generations of ocean iron cycle models, which would, in turn, provide an opportunity to update our understanding of how sedimentary iron supply impacts the ocean carbon cycle (2). Optimal conditions for sedimentary cFe input in the ocean may be predicted, firstly, by considering the known surface exchangeable (0-1 cmbsf) inventory of porewater Fe bearing crustal isotope compositions (Fig. 7a). Large differences exist in the dFe isotopic signature of surface exchangeable porewater in the upper 1500m of the ocean with a tendency towards light values that are attributable to the variable influence of reductive and non-reductive sediment dissolution. By contrast the isotopic signatures from equivalent porewater depths are far more uniform and crustal in ocean sediments beneath 1500m due to the lithogenic production of cFe in oxic-nitrogenous zones. These sites also correspond to low benthic oxygen consumption rates (<2 mmol m^{-2} d^{-1}) sufficient to supress the generation of sFe by RD in ferruginous zones well below the sediment-water interface. Secondly, the entrainment potential for cFe is illustrated by comparing compilations of benthic O_2 flux (sediment community O_2 consumption rates (65)) and the benthic nepheloid inventories observed in bottom water (29) (Fig. 7b). Sediments below 1500m water depth exhibit the lowest rates of O_2 consumption, almost exclusively <2 mmol m^{-2} d^{-1}, so that they are most likely to contain exchangeable porewater inventories of lithogenic cFe (*c.f.* Fig. 7a). Bottom waters bearing the highest benthic nepheloid inventories are also found in deep waters, notably in western margins and basins of the North and South Atlantic Ocean, indicating that these regions could optimise the entrainment of cFe and lithogenic isotopes in the ocean. Shelf and slope sediments above 1500m, show the highest benthic fluxes of O_2, consistent with these regions supporting reservoirs of reduced, soluble and light Fe isotopes in porewaters that can be exchanged with the upper ocean (7, 11). A high degree of variation to benthic nepheloid inventories and oxygen flux (<1 to >10 mmol m^{-2} d^{-1}) is also shown in sediments above 1500m (Fig. 7b) and suggests the relative contributions of RD and NRD might vary considerably between regions of the upper ocean.

Further localised and seasonal variations in sediment dissolution and mechanisms of entrainment are certain to exist, particularly close to margins, that are not represented by the data or grid resolution presented here. The exchangeable inventories of cFe in oxidising porewaters will also respond to the underlying influence of igneous provenance and OC (*c.f.* Fig. 2b), which we have not explicitly accounted for. Therefore, the broader implications of our findings are potentially significant but not yet known. The stability of organo-mineral Fe colloids means they may not succumb to the same fate (rapid precipitation, aggregation, and removal) that limits the extent to which reductive Fe inputs influence the ocean interior. By the same token, the bioavailability of these organo-mineral Fe colloids is unknown, and begs the question: Is there a trade-off between the endurance of Fe colloids in the ocean and their accessibility for phytoplankton? An additional, more stable source of dFe deeper in the water column governed by lithogenic colloid production, which has been ignored in our earlier numerical and conceptual models of the iron cycle, will contribute to the buffering of the ocean dFe inventory against variability from other sources and lower further the mean residence time of dFe.

Conclusions

South Atlantic Sediments contain a non-linear down slope gradient in O_2 consumption rates, with coupled porewater depth zonation of nitrous oxide, Mn oxide, and Fe oxide reduction pathways, which are consistent with anticipated down-slope gradients in OC flux and decomposition at the ocean floor. Porewater maxima in dissolved Fe contents have light Fe isotopic composition in the form of mostly soluble Fe species, reflecting the reductive-dissolution of Fe(III) to Fe(II) by bacteria in ferruginous zones. Beneath these maxima in dissolved Fe contents, heavy dissolved Fe isotopes corresponded to the reactive loss of soluble Fe(II) with free sulphide. Detectable amounts of dissolved Fe in the overlying oxic-nitrogenous zones have dissolved Fe isotope compositions that are indistinguishable from average igneous weathering products due to the production of Fe colloids from lithogenic weathering. Based on a strong correlation between colloidal Fe abundance and TOC, we propose colloidal Fe stability may be promoted by Fe(oxyhydr)oxide adsorption to OC and the formation of nano-scale ferrihydrite organo-mineral composites.

Modelled porewater production and consumption profiles indicate that a soluble Fe pool of Fe(II) accounts for the light isotopic composition of ferruginous zones, whereas dissolved Fe and its isotope composition was mostly determined by the genesis of colloidal Fe in overlying oxic-nitrogenous zones of marine sediments. Our isotopically-constrained model experiments show that non-reductive weathering of lithogenic material is required to account for the widespread occurrence of colloidal Fe in porewater – oxidative conversion of soluble Fe(II) to colloidal Fe(III) alone, was an insufficient explanation for the presence of Fe colloids and their isotope composition, as were alternative authigenic mineral or ligand-stabilised “sinks” for soluble Fe(II) supplied by reductive dissolution.

We determine that oxic-nitrogenous ocean sediments are sites of lithogenic weathering and organo-mineral formation that will be provide a “rusty source” of colloidal Fe throughout the global ocean. Coupled to the generation of benthic nepheloid inventories, oxidising sediments will be important sites for benthic Fe exchange that need to be reappraised for their role in ocean biogeochemical cycles.

Materials and methods

A Bowers Connelly Mega Corer collected multiple intact surface sediment cores from 6 sites in the South Atlantic during occupation by the RRS *James Cook* (JC068) in 2011. All cores were transferred to a controlled temperature laboratory replicating bottom water conditions (4-8°C) for microsensor profiling and porewater extraction, where all apparatus in contact with the samples (syringes, Teflon, centrifuge tubes and Low-Density Polyethylene (LDPE) bottles were cleaned prior to use (72 hours in 10% Decon; 72 hours in 6M HCl; 72 hours in 6M HNO_3; rinsed by 18.2MΩ deionised water).

Microsensor determinations of dissolved oxygen were performed by a Unisense micro-profiling suite of apparatus following analytical procedures previously described and used in coastal and deep-sea sediments elsewhere (7, 9, 28). Oxygen penetration depths were either measured directly in the upper 6cm or estimated from model fits to steady state oxygen consumption rates as previously described (7, 9).

Rhizon samplers (2.5 x 50 mm "CSS" type, Rhizosphere Research Products) were inserted at 1cm depth intervals through pre-drilled holes into a second sediment core recovered from the Mega Core deployment. Porewater was filtered (~0.15 μm) by suction through each Rhizon into a BD Discardit syringe in an ambient atmosphere. Sample aliquots (2 ml) were diluted 15-fold by 18.2 MΩ deionised water and stored in the dark prior to ship-board nutrient analyses (NO_3^-, NO_2^-, NH_4^+) by a 5-channel Bran and Luebbe AAIII segmented flow colorimetric auto analyser after Homoky et al. (9) and previously reported by Bridgestock *et al.* (66).

Under a nitrogen atmosphere, a third sediment core was extruded, sliced at 1cm depth intervals, and centrifuged at 9,000*g* for 6 minutes, before supernatant porewaters were siphoned through Teflon tubes into BD Discardit syringes. Samples for dissolved metals were passed through Whatmann Puradisc 25 syringe filters with polyethersulphone membranes (0.2 μm) and selected sub-samples for soluble metals were passed through a second, in-line Whatman Anatop 25 syringe filter with aluminium oxide membrane (0.02 μm). All porewater samples were later acidified to pH<2 by adding 6 μl of 6M quartz distilled (Q) HCl per millilitre of sample and stored refrigerated prior to analyses.

Sediment residues from centrifugation were freeze dried under vacuum and later pulverised in an agate pestle and mortar for carbon, and opal determinations. The bulk composition of sediment cores is described by dry-mass measurements of the total carbonate ($CaCO_3$), total organic carbon (TOC), opal and - by difference from the total dry mass - lithogenic material. The difference between coulometric determination (UIC 5012 Coulometer) of total carbon (TC) and total inorganic carbon (TIC) content of powdered sediments were used to calculate TOC. TC was calculated from CO_2 released during sample combustion, and TIC was calculated from CO_2 released during heated sample reaction with 1.5 M H_3PO_4. Accuracy of TC and TIC determinations was assessed with anhydrous $CaCO_3$ powder, with a mean recovery of 100.4±0.8% (1SD, *n*=15). The limit of detection (LOD = 3SD of blanks) was 10 mg C, equivalent to 0.03 wt% TOC. Opal content was measured by molybdate blue spectrometry on Si extracted solutions from dry homogenized sediments following the sodium bicarbonate sequential leaching method according to Mortlock and Froelich (67). Accuracy of opal determination was assessed by multiple analyses of a laboratory bulk sediment at the School of Geosciences, University of Edinburgh with a reproducibility of 1.54%.

A Thermo Scientific Element X2 Inductively Coupled Plasma-Mass Spectrometer (ICP-MS) was used to determine the concentration of aqueous metals in acidified porewater samples and sediment digests following Homoky *et al.* (9) and previously reported by Bridgestock *et al* (66). Briefly, porewaters were diluted 100-fold with 0.48 M Q-HNO_3, and external calibration standards were matrix matched to samples with 1% of the seawater standard NASS-5 (National Research Council Canada). The mass of ^{45}Sc spiked to all samples was used as an internal standard to monitor and correct for a reduction in signal intensity of over time. Accuracy of the method was verified by the intermittent analysis of blank-bracketed SLRS-5 (National Research Council Canada) within certified values, with a

RSD of 1.1 and 1.3% for Fe and Mn respectively. The LOD (3SD of analytical blanks, *n*=9) for reported Fe and Mn were 1 and 0.1 nmol l^{-1}, and procedural blanks were below these limits of detection.

Dissolved Fe isotopic compositions from porewaters were measured following previously published methods (9, 68). Aliquots of porewater containing Fe inventories from 20 to 104 ng were spiked with an ^{57}Fe-^{58}Fe double spike (in a 1:2 sample:spike ratio), evaporated to dryness in 7 mL Savillex^{TM} PFA Teflon vials, and then re-dissolved in 5 M quartz-distilled HCl + 0.001% v/v Optima H_20_2 before being passed through 135 μL AGMP-1 column purification. Fe was eluted from the columns in 0.8 mL of 1M quartz-distilled HCl and evaporated to dryness before being re-dissolved in 0.5 mL of 0.1 M Teflon-distilled HNO_3 for analysis by Multi Collector (MC)-ICPMS. Procedural blanks for this method have previously been shown to be 3 ng of Fe per sample (9). Samples were then analysed for Fe isotopic composition by Thermo Neptune MC-ICPMS with jet interface at the University of South Carolina, using an ESI Apex-Q introduction system, Pt Jet and Al X cones, following methods identical to those described previously (9). Fe isotopic compositions ($\delta^{56}Fe$) are expressed in typical delta notion relative to the IRMM-014 international Fe standard. The accuracy of this procedure has been previously demonstrated on seawater samples (68, 69), and here we assign 0.05‰ as an estimate of external precision of analysis, based on duplicate measurements of 60 GA10 seawater samples (0.1-1.8 nmol kg^{-1}), measured over multiple analytical sessions during the same time interval (69). In cases where the 2 standard internal error is larger than 0.05‰, we consider the 2SE a more representative estimate of uncertainty.

Acknowledgments

We thank the captain and crew of the *RRS James Cook* expedition JC068, and science party of UK-GEOTRACES GA10W. In particular Deborah Hembury and Yu-Te Hsieh (University of Oxford) for shipboard sampling assistance, Malcolm Woodward (Plymouth Marine Laboratory) for shipboard nutrient analyses, and Alex Thomas (University of Edinburgh) for supporting opal analyses by FD. RAM supported WBH for the collection of sediments and porewater and analyses of oxygen, metals and carbon through NERC grants (NE/F017197/1 and NE/H004394/1). WBH was independently supported by a NERC fellowship at University of Oxford (NE/K009532/1) to prepare samples for Fe isotope analyses and perform model experiments, and by a University Academic Fellowship at University of Leeds to write the manuscript. Fe isotope analyses by TMC and SGJ were supported by the University of South Carolina. DK and AT were funded by European Research Council under the European Union's Horizon 2020 research and innovation program (grant agreement 724289).

References

1. V. A. Elrod, W. M. Berelson, K. H. Coale, K. S. Johnson, The flux of iron from continental shelf sediments: a missing source for global budgets. *Geophys Res Lett* **31**, L12307 (2004).
2. A. Tagliabue, O. Aumont, L. Bopp, The impact of different external sources of iron on the global carbon cycle. *Geophysical Research Letters* **41**, 920-926 (2014).
3. W. B. Homoky *et al.*, Quantifying trace element and isotope fluxes at the ocean–sediment boundary: a review. *Philosophical Transactions of the Royal Society A: Mathematical, Physical and Engineering Sciences* **374** (2016).
4. A. Tagliabue *et al.*, How well do global ocean biogeochemistry models simulate dissolved iron distributions? *Global Biogeochemical Cycles* **30**, 149-174 (2016).

5. S. Severmann, C. M. Johnson, B. L. Beard, J. McManus, The effect of early diagenesis on the Fe isotope compositions of porewaters and authigenic minerals in continental margin sediments. *Geochimica et Cosmochimica Acta* **70**, 2006-2022 (2006).
6. W. B. Homoky, S. Severmann, R. A. Mills, P. J. Statham, G. R. Fones, Pore-fluid Fe isotopes reflect the extent of benthic Fe redox recycling: Evidence from continental shelf and deep-sea sediments. *Geology* **37**, 751-754 (2009).
7. J. K. Klar *et al.*, Stability of dissolved and soluble Fe(II) in shelf sediment pore waters and release to an oxic water column. *Biogeochemistry* 10.1007/s10533-017-0309-x, 1-19 (2017).
8. A. Radic, F. Lacan, J. W. Murry, Iron isotopes in the seawater of the equatorial Pacific Ocean: New constraints for the oceanic iron cycle. *Earth and Planet. Sci. Lett.* **306**, 1-10 (2011).
9. W. B. Homoky, S. G. John, T. Conway, R. A. Mills, Distinct iron isotopic signatures and supply from marine sediment dissolution. *Nature Communications* **4** (2013).
10. I. Rapp *et al.*, El Niño-Driven Oxygenation Impacts Peruvian Shelf Iron Supply to the South Pacific Ocean. *Geophysical Research Letters* **47**, e2019GL086631 (2020).
11. S. Severmann, J. McManus, W. M. Berelson, D. E. Hammond, The continental shelf benthic iron flux and its isotope composition. *Geochimica et Cosmochimica Acta* **74**, 3984-4004 (2010).
12. W. B. Homoky *et al.*, Dissolved oxygen and suspended particles regulate the benthic flux of iron from continental margins. *Marine Chemistry* **134-135**, 59-70 (2012).
13. S. G. John, J. Mendez, J. Moffett, J. Adkins, The flux of iron and iron isotopes from San Pedro Basin sediments. *Geochimica et Cosmochimica Acta* **93**, 14-29 (2012).
14. A. Noffke *et al.*, Benthic iron and phosphorous fluxes across the Peruvian oxygen minimum zone. *Limnol. Oceanogr.* **57**, 851-867 (2012).
15. M. Staubwasser, R. Schoenberg, F. von Blanckenburg, S. Krüger, C. Pohl, Isotope fractionation between dissolved and suspended particulate Fe in the oxic and anoxic water column of the Baltic Sea. *Biogeosciences* **10**, 233-245 (2013).
16. P. J. Lam, M. I. Heller, P. E. Lerner, J. W. Moffett, K. N. Buck, Unexpected Source and Transport of Iron from the Deep Peru Margin. *ACS Earth and Space Chemistry* **4**, 977-992 (2020).
17. F. Scholz, S. Severmann, J. McManus, C. Hensen, Beyond the Black Sea paradigm: The sedimentary fingerprint of an open-marine iron shuttle. *Geochimica et Cosmochimica Acta* **127**, 368-380 (2014).
18. A. W. Dale *et al.*, A revised global estimate of dissolved iron fluxes from marine sediments. *Global Biogeochemical Cycles* **29**, 691-707 (2015).
19. J. J. Middelburg, K. Soetaert, P. M. J. Herman, Empirical relationships for use in global diagenetic models. *Deep Sea Research Part I: Oceanographic Research Papers* **44**, 327-344 (1997).
20. T. M. Conway, S. G. John, Quantification of dissolved iron sources to the North Atlantic Ocean. *Nature* **511**, 212-215 (2014).
21. M. Labatut *et al.*, Iron sources and dissolved-particulate interactions in the seawater of the Western Equatorial Pacific, iron isotope perspectives. *Global Biogeochemical Cycles* **28**, 1044-1065 (2014).
22. C. Abadie, F. Lacan, A. Radic, C. Pradoux, F. Poitrasson, Iron isotopes reveal distinct dissolved iron sources and pathways in the intermediate versus deep Southern Ocean. *Proceedings of the National Academy of Sciences* **114**, 858-863 (2017).
23. J. N. Fitzsimmons *et al.*, Partitioning of dissolved iron and iron isotopes into soluble and colloidal phases along the GA03 GEOTRACES North Atlantic Transect. *Deep Sea Research Part II: Topical Studies in Oceanography* **116**, 130-151 (2015).
24. R. Schlitzer *et al.*, The GEOTRACES Intermediate Data Product 2017. *Chemical Geology* **493**, 210-223 (2018).

25. K. Kuma, A. Katsumoto, J. Nishioka, K. Matsunaga, Size-fractionated iron concentrations and Fe(III) hydroxide solubilities in various coastal waters. *Estuarine, Coastal and Shelf Science* **47**, 275-283 (1998).
26. K. Dideriksen, J. A. Baker, S. L. S. Stipp, Fe isotope fractionation between inorganic aqueous Fe(III) and a Fe siderophore complex. *Mineral Mag* **72**, 313-316 (2008).
27. K. Kunde *et al.*, Iron Distribution in the Subtropical North Atlantic: The Pivotal Role of Colloidal Iron. *Global Biogeochemical Cycles* **n/a**.
28. W. B. Homoky *et al.*, Iron and Manganese diagenesis in deep sea volcanogenic sediments and the origins of pore water colloids. *Geochim. Cosmochim. Acta* **75**, 5032-5048 (2011).
29. W. D. Gardner, M. J. Richardson, A. V. Mishonov, Global assessment of benthic nepheloid layers and linkage with upper ocean dynamics. *Earth and Planetary Science Letters* **482**, 126-134 (2018).
30. J. C. Latimer, G. M. Filippelli, Sedimentary iron records from the Cape Basin. *Deep Sea Research Part II: Topical Studies in Oceanography* **54**, 2422-2431 (2007).
31. W. Weijer, M. E. Maltrud, W. B. Homoky, K. L. Polzin, L. R. M. Maas, Eddy-driven sediment transport in the Argentine Basin: Is the height of the Zapiola Rise hydrodynamically controlled? *Journal of Geophysical Research: Oceans* **120**, 2096-2111 (2015).
32. R. C. Thunell, Carbonate dissolution and abyssal hydrography in the Atlantic Ocean. *Marine Geology* **47**, 165-180 (1982).
33. T. J. Shaw, J. M. Gieskes, R. A. Jahnke, Early diagenesis in differing depositional environments: The response of transition metals in pore water. *Geochimica et Cosmochimica Acta* **54**, 1233-1246 (1990).
34. B. L. Beard *et al.*, Application of Fe isotopes to tracing the geochemical and biological cycling of Fe. *Chemical Geology* **195**, 87-117 (2003).
35. A. Dutkiewicz, R. D. Müller, S. O'Callaghan, H. Jónasson, Census of seafloor sediments in the world's ocean. *Geology* 10.1130/g36883.1 (2015).
36. R. N. Glud, Oxygen dynamics of marine sediments. *Marine Biology Research* **4**, 243-289 (2008).
37. P. N. Froelich *et al.*, Early oxidation of organic matter in pelagic sediments of the eastern equatorial Atlantic: suboxic diagenesis. *Geochimica et Cosmochimica Acta* **43**, 1075-1090 (1979).
38. S. Henkel, S. Kasten, J. F. Hartmann, A. Silva-Busso, M. Staubwasser, Iron cycling and stable Fe isotope fractionation in Antarctic shelf sediments, King George Island. *Geochimica et Cosmochimica Acta* **237**, 320-338 (2018).
39. S. Henkel, S. Kasten, S. W. Poulton, M. Staubwasser, Determination of the stable iron isotopic composition of sequentially leached iron phases in marine sediments. *Chemical Geology* **421**, 93-102 (2016).
40. L. Wu, B. L. Beard, E. E. Roden, C. M. Johnson, Stable Iron Isotope Fractionation Between Aqueous Fe(II) and Hydrous Ferric Oxide. *Environmental Science & Technology* **45**, 1847-1852 (2013).
41. B. L. Beard *et al.*, Iron isotope fractionation between aqueous ferrous iron and goethite. *Earth and Planetary Science Letters* **295**, 241-250 (2010).
42. A. J. Birchill *et al.*, Seasonal iron depletion in temperate shelf seas. *Geophysical Research Letters* **44**, 8987-8996 (2017).
43. M. Gledhill, K. N. Buck, The organic complexation of iron in the marine environment: a review. *Frontiers in Microbiology* **3**, 1-17 (2012).
44. P. H. Santschi, Marine colloids, agents of the self-cleansing capacity of aquatic systems: Historical perspective and new discoveries. *Marine Chemistry* **207**, 124-135 (2018).
45. M. L. Wells, E. D. Goldberg, Marine submicron particles. *Marine Chemistry* **40**, 5-18 (1992).

46. R. Raiswell, D. E. Canfield, The Iron Biogeochemical Cycle Past and Present. *Geochemical Perspectives* **1**, 1-2 (2012).

47. C. van der Zee, D. R. Roberts, D. G. Rancourt, C. P. Slomp, Nanogoethite is the dominant reactive oxyhydroxide phase in lake and marine sediments. *Geology* **31**, 993-996 (2003).

48. A. Gartman, A. J. Findlay, G. W. Luther, Nanoparticulate pyrite and other nanoparticles are a widespread component of hydrothermal vent black smoker emissions. *Chemical Geology* **366**, 32-41 (2014).

49. A. D. Anbar, O. Rouxel, Metal Stable Isotopes in Paleoceanography. *Annual Review of Earth and Planetary Sciences* **35**, 717-746 (2007).

50. E. Lotfi-Kalahroodi *et al.*, Iron isotope fractionation in iron-organic matter associations: Experimental evidence using filtration and ultrafiltration. *Geochimica et Cosmochimica Acta* **250**, 98-116 (2019).

51. M. T. Jones *et al.*, Quantifying the impact of riverine particulate dissolution in seawater on ocean chemistry. *Earth and Planetary Science Letters* **395**, 91-100 (2014).

52. C. Jeandel, Overview of the mechanisms that could explain the ‘Boundary Exchange’ at the land–ocean contact. *Philosophical Transactions of the Royal Society A: Mathematical, Physical and Engineering Sciences* **374**, 20150287 (2016).

53. L. K. ThomasArrigo, J. M. Byrne, A. Kappler, R. Kretzschmar, Impact of Organic Matter on Iron(II)-Catalyzed Mineral Transformations in Ferrihydrite–Organic Matter Coprecipitates. *Environmental Science & Technology* **52**, 12316-12326 (2018).

54. K. Lalonde, A. Mucci, A. Ouellet, Y. Gélinas, Preservation of organic matter in sediments promoted by iron. *Nature* **483**, 198-200 (2012).

55. K. A. Lettmann *et al.*, Estimation of biogeochemical rates from concentration profiles: A novel inverse method. *Estuarine, Coastal and Shelf Science* **100**, 26-37 (2012).

56. K. Laufer, H. Røy, B. B. Jørgensen, A. Kappler, Evidence for the Existence of Autotrophic Nitrate-Reducing Fe(II)-Oxidizing Bacteria in Marine Coastal Sediment. *Applied and Environmental Microbiology* **82**, 6120 (2016).

57. C. M. Johnson, E. E. Roden, S. A. Welch, B. L. Beard, Experimental constraints on Fe isotope fractionation during magnetite and Fe carbonate formation coupled to dissimilatory hydrous ferric oxide reduction. *Geochimica et Cosmochimica Acta* **69**, 963 (2005).

58. L. Wu, G. Druschel, A. Findlay, B. L. Beard, C. M. Johnson, Experimental determination of iron isotope fractionations among ,Fe2+(aq)-FeS(aq)-Mackinawite at low temperatures: Implications for the rock record. *Geochimica et Cosmochimica Acta* **89**, 46-61 (2012).

59. S. M. Kraemer, Iron oxide dissolution and solubility in the presence of siderophores. *Aquatic Sciences* **66**, 3-18 (2004).

60. J. G. Wiederhold *et al.*, Iron Isotope Fractionation during Proton-Promoted, Ligand-Controlled, and Reductive Dissolution of Goethite. *Environmental Science & Technology* **40**, 3787-3793 (2006).

61. C. B. Kennedy, S. D. Scott, F. G. Ferris, Hydrothermal phase stabilization of 2-line ferrihydrite by bacteria. *Chemical Geology* **212**, 269-277 (2004).

62. F. Couceiro *et al.*, Impact of resuspension of cohesive sediments at the Oyster Grounds (North Sea) on nutrient exchange across the sediment–water interface. *Biogeochemistry* **113**, 37-52 (2013).

63. D. A. Cacchione, W. D. Grant, D. E. Drake, S. M. Glenn, Storm-Dominated Bottom Boundary Layer Dynamics on the Northen California Continental Shelf: Measurements and Predictions. *Journal of Geophysical Research* **92**, 1817-1827 (1987).

64. D. A. Cacchione, L. F. Pratson, A. S. Ogston, The Shaping of Continental Slopes by Internal Tides. *Science* **296**, 724 (2002).

65. T. Stratmann, K. Soetaert, C.-L. Wei, Y.-S. Lin, D. van Oevelen, The SCOC database, a large, open, and global database with sediment community oxygen consumption rates. *Scientific Data* **6**, 242 (2019).
66. L. Bridgestock *et al.*, Controls on the barium isotope compositions of marine sediments. *Earth and Planetary Science Letters* **481**, 101-110 (2018).
67. R. A. Mortlock, P. N. Froelich, A simple method for the rapid determination of biogenic opal in pelagic marine sediments. *Deep Sea Research Part A. Oceanographic Research Papers* **36**, 1415-1426 (1989).
68. T. M. Conway, A. D. Rosenberg, J. F. Adkins, S. G. John, A new method for precise determination of iron, zinc and cadmium stable isotope ratios in seawater by double-spike mass spectrometry. *Analytica Chimica Acta* **793**, 44-52 (2013).
69. T. M. Conway, S. G. John, F. Lacan, Intercomparison of dissolved iron isotope profiles from reoccupation of three GEOTRACES stations in the Atlantic Ocean. *Marine Chemistry* **183**, 50-61 (2016).
70. C. M. Johnson, E. E. Roden, S. A. Welch, B. L. Beard, Experimental constraints on Fe isotope fractionation during magnetite and Fe carbonate formation coupled to dissimilatory hydrous ferric oxide reduction. *Geochimica et Cosmochimica Acta* **69**, 963-993 (2005).

Figure legends.

Figure 1. The location and core-top composition of sediment samples from GA10W. A blue colour index shows 500 m water depth intervals in a plan view (top) of the study region and a section view (bottom) along the GA10W sample transect. Sediment classifications of stations 8-23 include cohesive silts-clays, whereas station 24 is a non-cohesive permeable sand. Station 18 lies well beneath the likely Carbonate Compensation Depth (CCD). Pie charts indicate the mean surface (0-5 cmbs) proportions of lithogenic and pelagic components between all sites (SI Appendix, Tables S1and S2).

Figure 2. (a) Porewater concentrations of dFe verses cFe. Error bars (±2sigma) are typically within the size of individual data markers. Discrete observations from oxic-nitrogenous zones fall along a 1:1 line due to the high relative abundance of cFe. dFe exceeds cFe concentrations in underlying ferruginous zones due to the low relative abundance of cFe in these regions of the sediment. Concentrations of cFe span 3 orders of magnitude in porewater oxic-nitrogenous zones across all sites and exceed the concentrations of ocean bottom water (24), **(b) Mean porewater cFe concentration verses mean total organic carbon (TOC) in core top sediments (0-5cmbsf).** A dashed black line shows a significant linear fit through GA10W sites ($r = 0.962$, $p = 0.038$). Values from mafic volcanic sediments in the Southern Ocean (28), indicate that additional factors other than TOC also control the abundance of cFe in porewater, such as lithogenic provenance.

Figure 3. The relationship between δ^{56}dFe and relative abundance of cFe in ocean sediment porewater. Values compiled from the South Atlantic (this study sites 18, 21 and 22), and previous studies by (a) Homoky *et al.* (6) and (b) Klar *et al.* (7). Error bars (±2sigma) are within the size of individual data markers. The grey bar indicates the average Fe isotopic composition of crustal rocks.

Figure 4. Modelled porewater Fe production rate profiles. Comparison of measured sFe and dFe with REC model fits to observations across the oxic/nitrogenous-ferruginous transition of GA10W station 21. The concentrations and production rates of cFe are calculated by model difference (cFe = dFe-sFe).

Figure 5. Porewater sFe and cFe isotope mass-balance experiments. Summary of results in which porewater dFe isotope compositions are simulated by two idealised controls on the sFe and cFe isotope reservoirs: Firstly, the isotope fraction effect (α) attributed to sFe loss (e.g. oxidation), and secondly, the origin of porewater cFe. The value of α is either >1 (a, c) as is commonly predicted for Fe(oxyhydr)oxide formation or <1 (b, d), as has been attributed to Fe (oxyhydr)oxide formation across some ocean chemoclines (15) and is predicted by some other (e.g. carbonate) mineral formations (70) and Fe(III)-ligand complexes (26). cFe is either an authigenic mineral supplied by sFe oxidation with a corresponding isotope composition (a, b), or cFe is supplied by non-reductive weathering of lithogenic material with crustal isotope compositions (c, d). In all scenarios, the resultant composition of dFe reflects the isotopic mass balance of sFe and cFe pools. Model equations are provided in the SI Appendix (SI Appendix, SI Text 1).

Figure 6. **A revised scheme of sedimentary iron supply depicting seven processes that may promote the exchange of lithogenic iron colloids (cFe) and isotopes to ocean interior.** (1) Production and diffusion of lithogenic cFe (depecited as cFeOOH(orgC)) in oxic-nitrogenous ocean sediment porewater; (2) Enhanced cFe production from dissolution of mafic minerals; (3) Enhanced cFe stablisation by organic C; (4) Porewater advection through permeable sediments of the continental shelf; (5) Entrainment by internal waves and density horizons; (6) Entrainments by a Benthic Boundary Layer (BBL) coupled to surface ocean EKE; (7) Entrainment by the Surface Mixed Layer (SML) and Island Mass Effects. Sedimentary release by reductive dissolution is restricted to shoaled porewater ferriclines beneath high organic matter flux or Oxygen Minimum Zones (OMZs) in the upper 1500m of the ocean, and rely on stabilisation by organic Ligands to resist secondary oxidation and precipitation from the water column.

Figure 7. (a) The isotopic signature of dissolved Fe in surface exchangeable sediment porewaters. Data markers correspond to measured surface values compiled from this study (SI Appendix, Table S5), the South Atlantic, Cape margin (9), the North Pacific, Oregon and California margins and Borderland Basins (6, 11), the North Atlantic, Celtic Sea (7), and the Southern Ocean, Crozet Island abyss (6). The measured surface inventory of porewater dFe is illustrated by the size of data markers, and the associated benthic flux (sediment consumption) of O_2 by the colour scale. **(b) The entrainment potential for colloidal Fe and lithogenic isotope signatures in the ocean.** Mean sediment community O_2 consumption rates complied by Stratmann *et al.* (65) are gridded here at 2 degrees and plotted using the same colour scale to data in (a). The suspended particle load in bottom waters reported by Gardner *et al.* (29) is reproduced with interpolated lines of equal concentration using means values from a 2-degree grid.

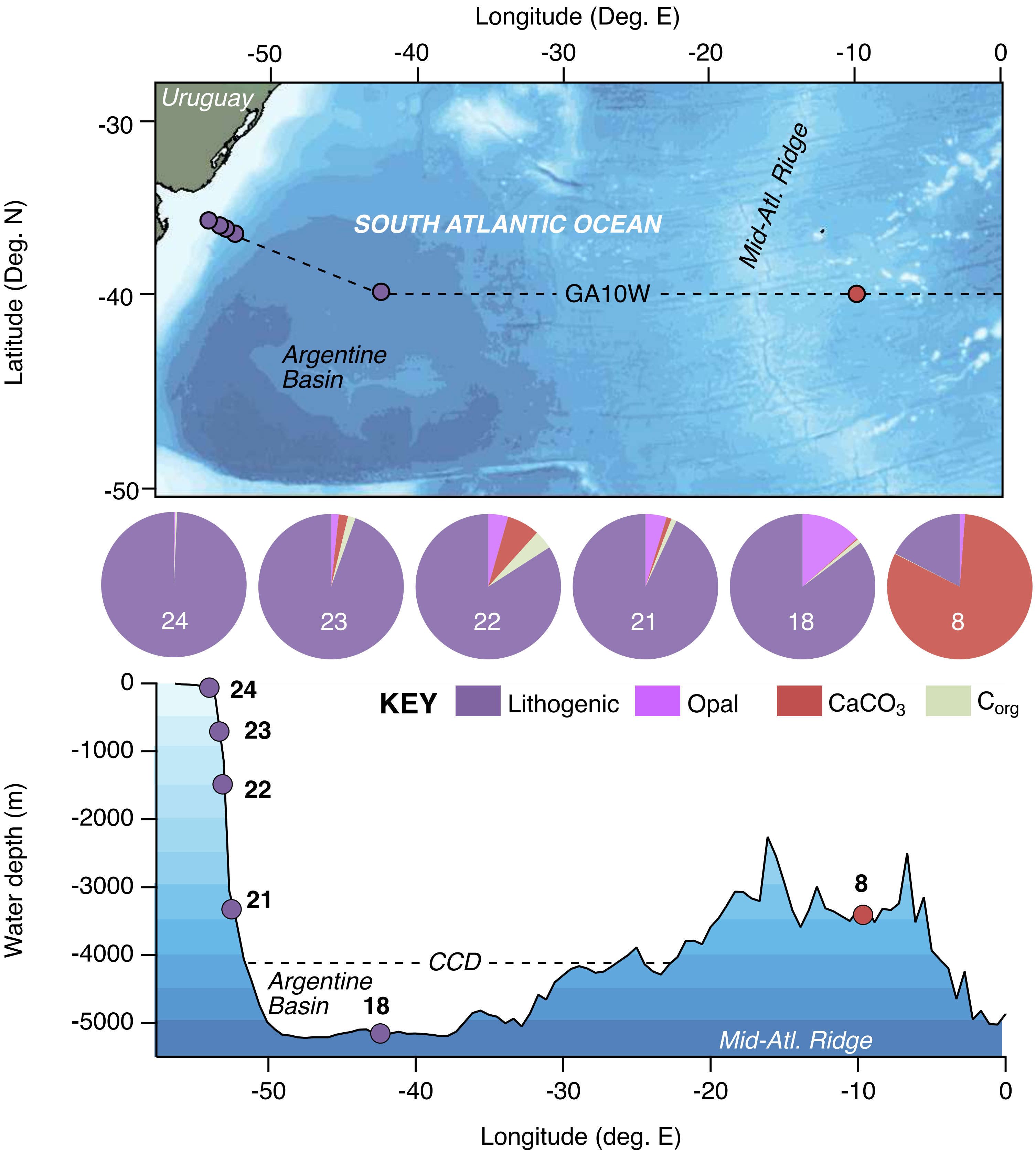
Longitude (Deg. E)
-50
-40
-30
-20
-10
0
-30
-40
-50
Latitude (Deg. N)
Uruguay
SOUTH ATLANTIC OCEAN
Mid-Atl. Ridge
GA10W
Argentine Basin
24
23
22
21
18
8
0
-1000
-2000
-3000
-4000
-5000
Water depth (m)
KEY
Lithogenic
Opal
$CaCO_3$
C_{org}
24
23
22
21
8
CCD
Argentine Basin
18
Mid-Atl. Ridge
-50
-40
-30
-20
-10
0
Longitude (deg. E)

Figure 1

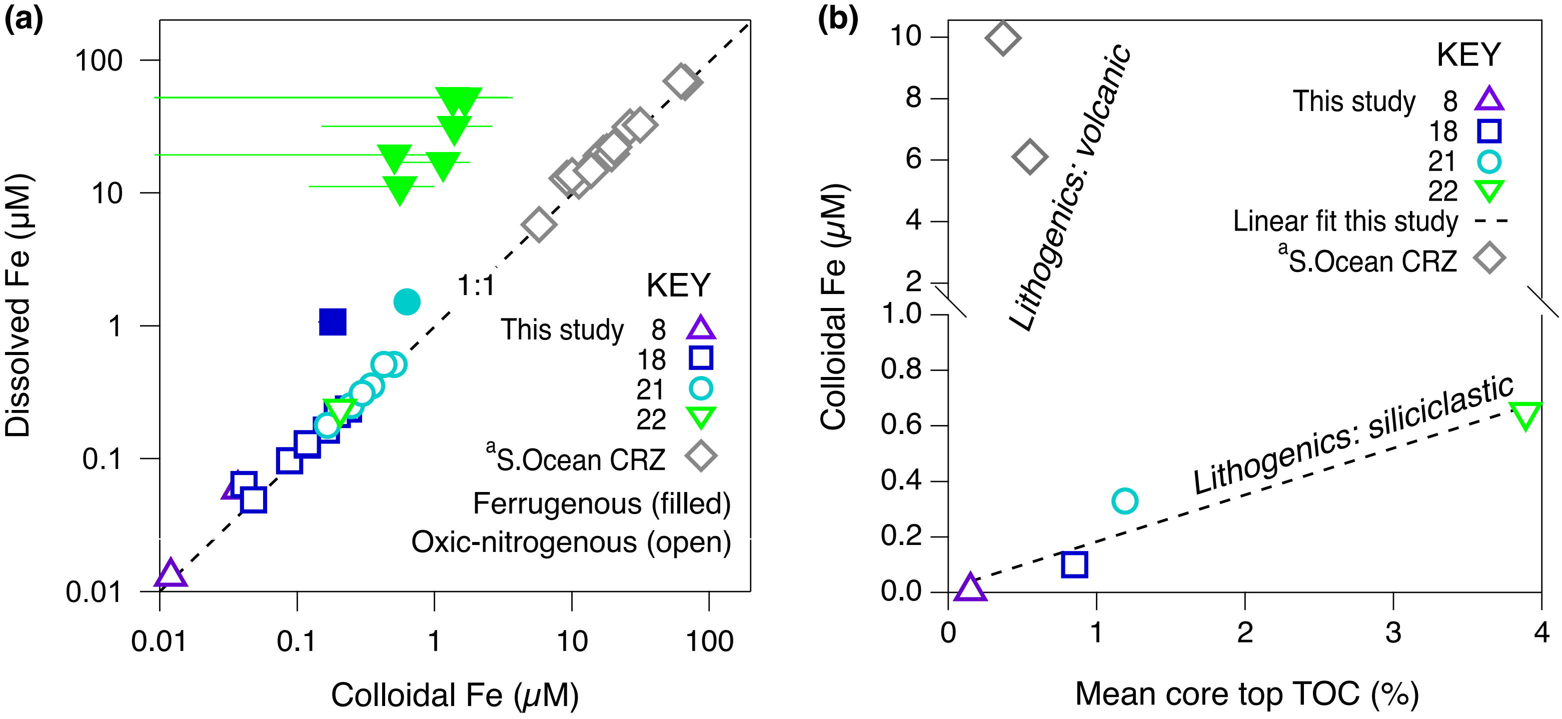
(a)
Dissolved Fe (μM)
Colloidal Fe (μM)
100
10
1
0.1
0.01
0.01
0.1
1
10
100
1:1
KEY
This study 8 △
18 □
21 ○
22 ▽
^{a}S.Ocean CRZ ◇
Ferrugenous (filled)
Oxic-nitrogenous (open)
(b)
Colloidal Fe (μM)
Mean core top TOC (%)
10
8
6
4
2
1.0
0.8
0.6
0.4
0.2
0.0
0
1
2
3
4
Lithogenics: volcanic
Lithogenics: siliciclastic
KEY
This study 8 △
18 □
21 ○
22 ▽
Linear fit this study - -
^{a}S.Ocean CRZ ◇

Figure 2

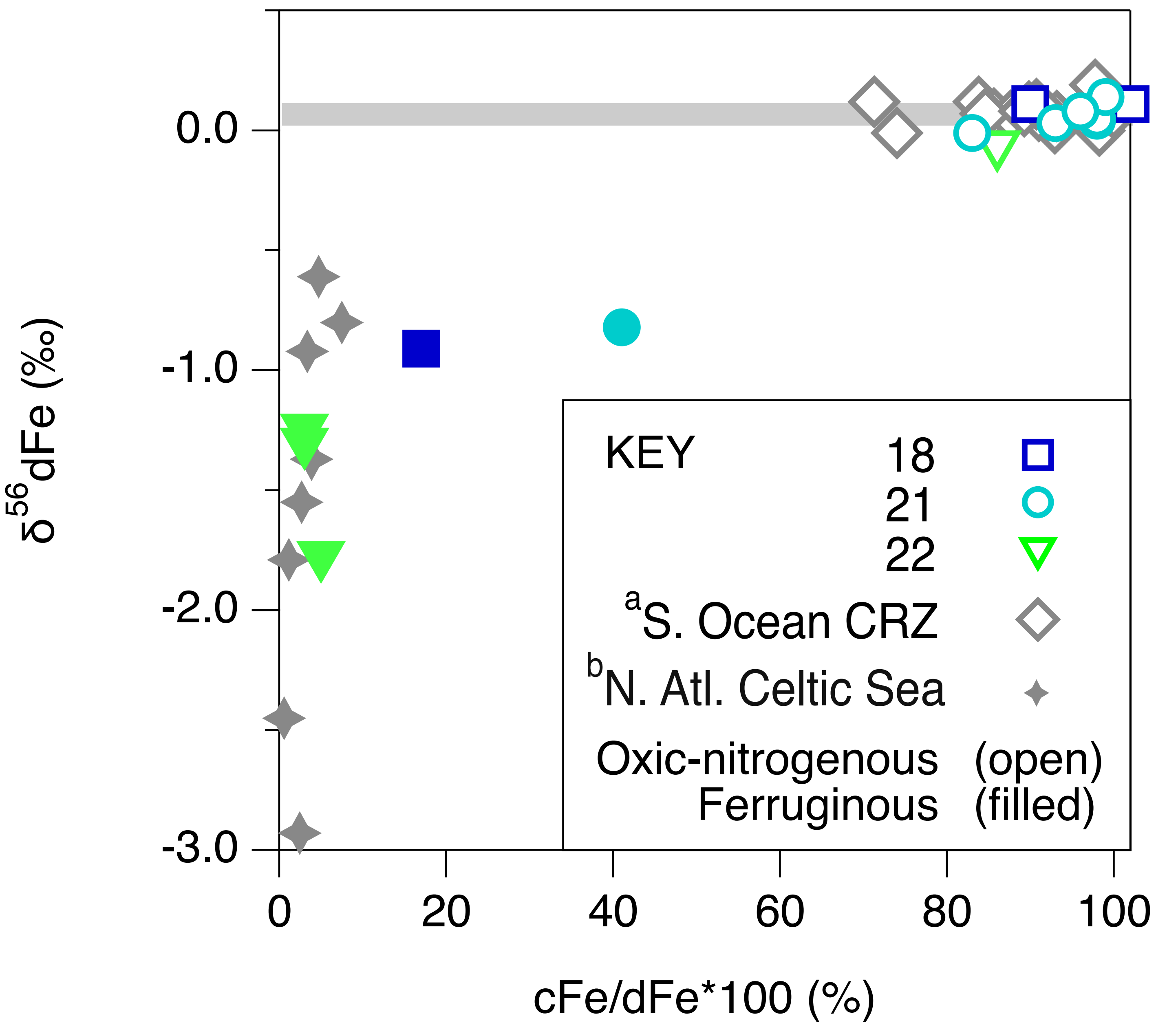
δ^{56}dFe (‰)
0.0
-1.0
-2.0
-3.0
0
20
40
60
80
100
cFe/dFe*100 (%)
KEY
18 □
21 ○
22 ▽
^{a}S. Ocean CRZ ◇
^{b}N. Atl. Celtic Sea ✦
Oxic-nitrogenous (open)
Ferruginous (filled)

Figure 3

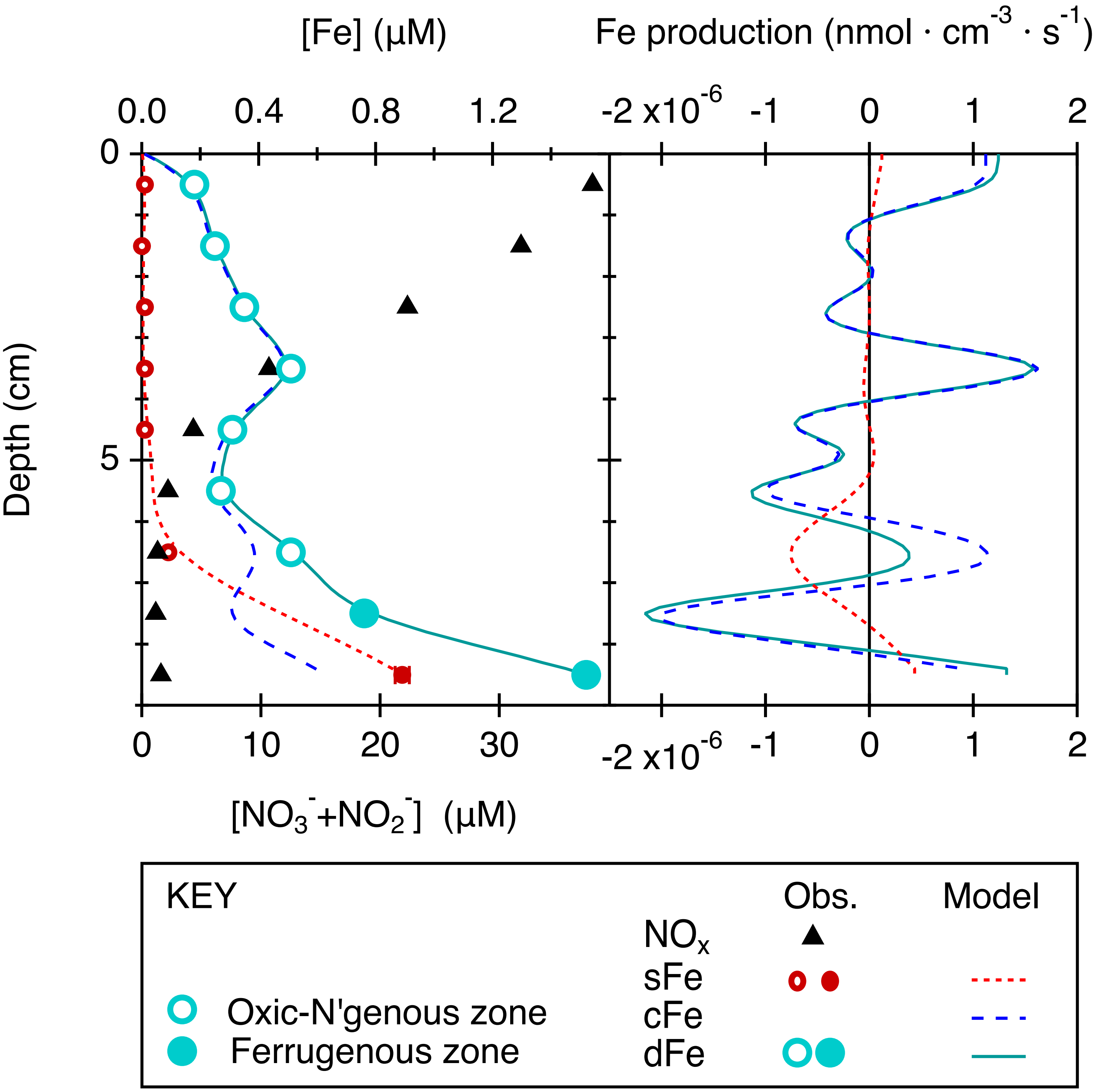
[Fe] (µM)
Fe production (nmol · cm-3 · s-1)
0.0
0.4
0.8
1.2
-2 x10-6
-1
0
1
2
Depth (cm)
0
5
0
10
20
30
[NO3-+NO2-] (µM)
KEY
Obs.
Model
NOx
sFe
cFe
dFe
Oxic-N'genous zone
Ferrugenous zone

Figure 4

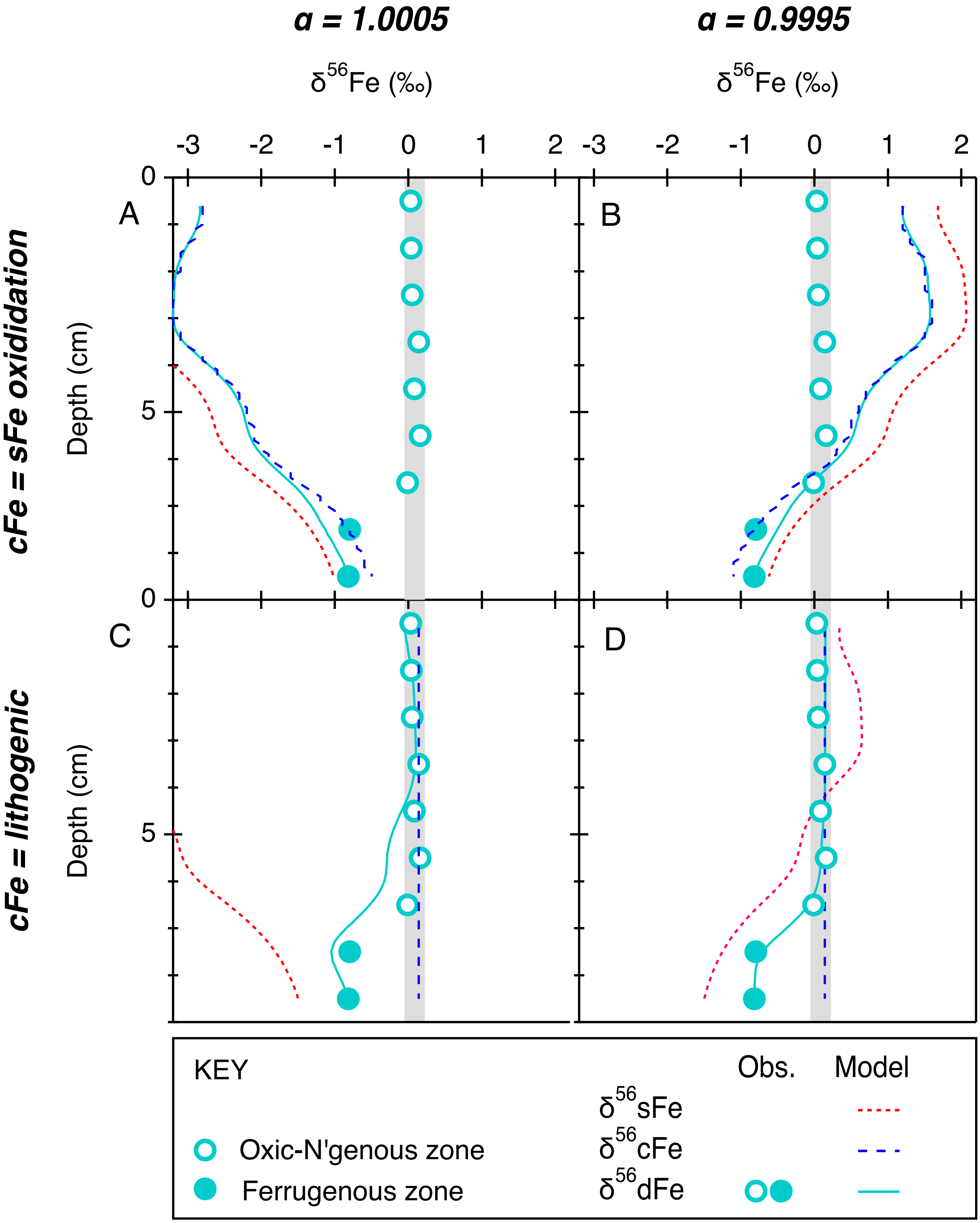
a = 1.0005
a = 0.9995
δ56Fe (‰)
δ56Fe (‰)
-3
-2
-1
0
1
2
0
5
0
5
A
B
C
D
cFe = sFe oxidation
cFe = lithogenic
Depth (cm)
Depth (cm)
KEY
Obs.
Model
δ56sFe
δ56cFe
δ56dFe
Oxic-N'genous zone
Ferrugenous zone

Figure 5

Figure 6

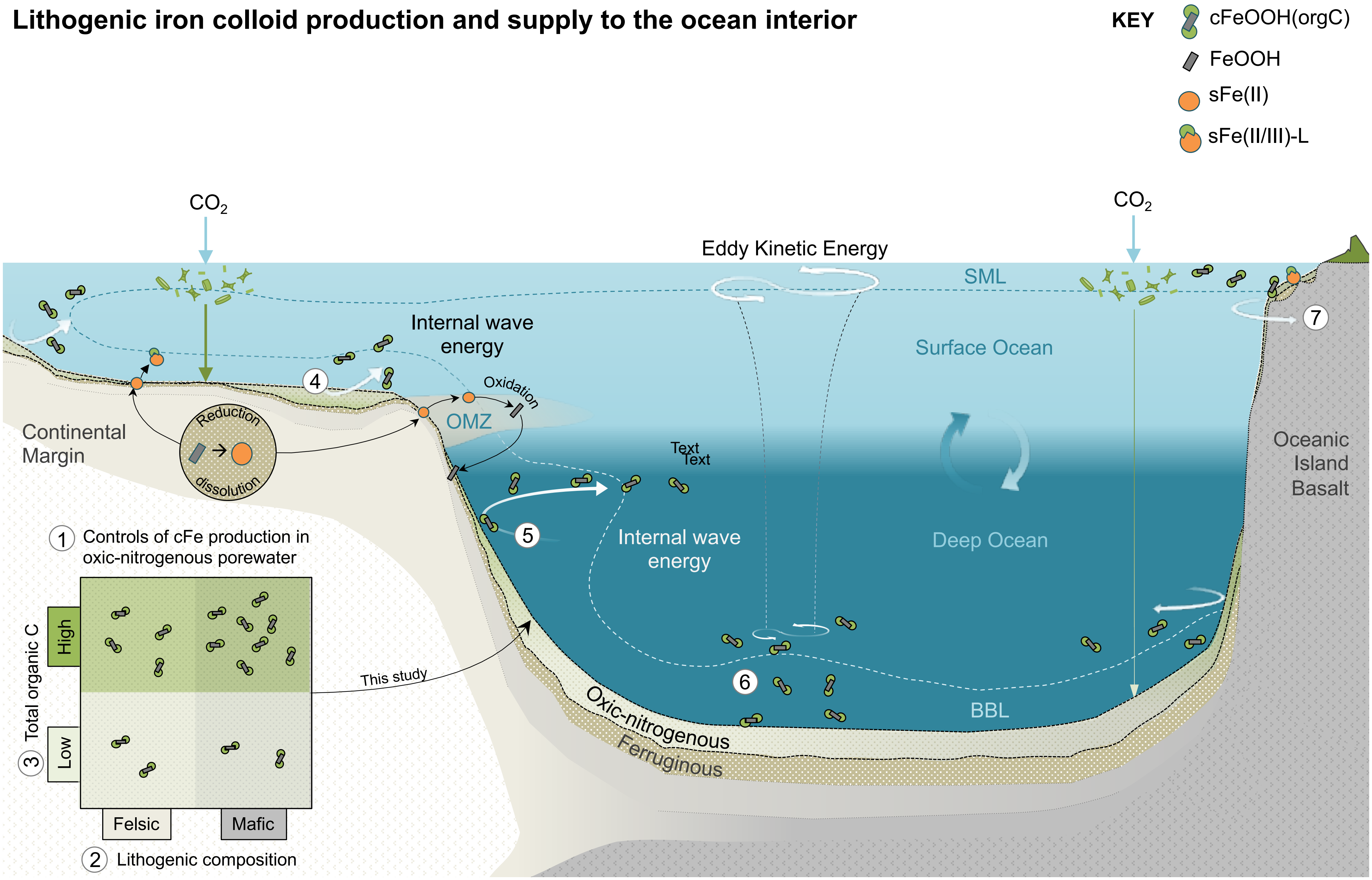
Lithogenic iron colloid production and supply to the ocean interior
KEY
cFeOOH(orgC)
FeOOH
sFe(II)
sFe(II/III)-L
CO_2
CO_2
Eddy Kinetic Energy
SML
Surface Ocean
Internal wave energy
4
Oxidation
OMZ
Reduction
dissolution
Continental Margin
Text
Text
5
Internal wave energy
Deep Ocean
Oceanic Island Basalt
7
1 Controls of cFe production in oxic-nitrogenous porewater
High
Low
3 Total organic C
Felsic
Mafic
2 Lithogenic composition
This study
6
BBL
Oxic-nitrogenous
Ferruginous

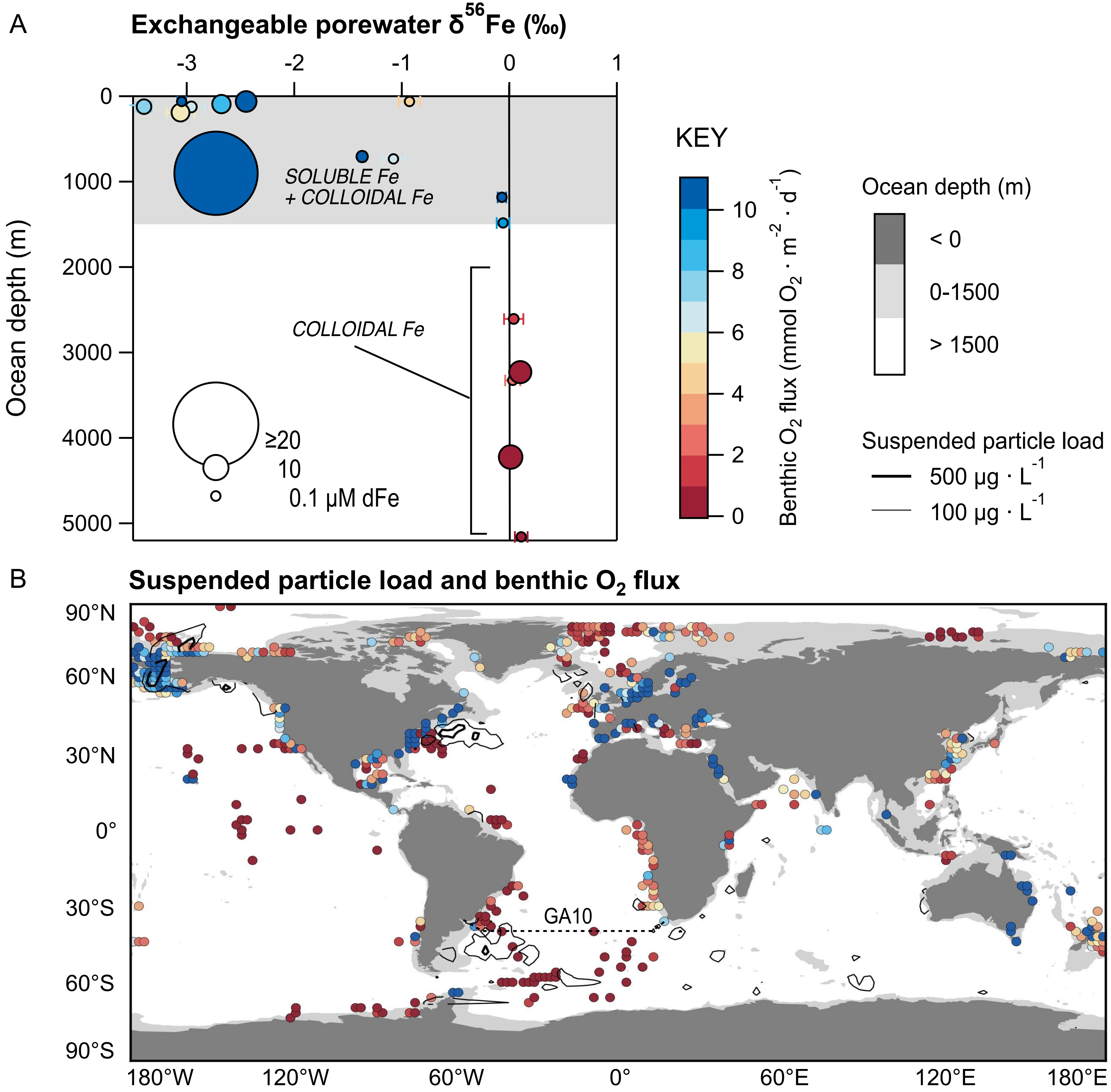
A
Exchangeable porewater δ56Fe (‰)
-3
-2
-1
0
1
0
1000
2000
3000
4000
5000
Ocean depth (m)
SOLUBLE Fe
+ COLLOIDAL Fe
COLLOIDAL Fe
≥20
10
0.1 µM dFe
KEY
10
8
6
4
2
0
Benthic O2 flux (mmol O2 · m-2 · d-1)
Ocean depth (m)
< 0
0-1500
> 1500
Suspended particle load
500 µg · L-1
100 µg · L-1
B
Suspended particle load and benthic O2 flux
90°N
60°N
30°N
0°
30°S
60°S
90°S
180°W
120°W
60°W
0°
60°E
120°E
180°E
GA10

Figure 7